An Approach to Yielding and Toughness in Rubber-Modified Thermoplastics

GIUSEPPE CIGNA,* CLAUDIO MAESTRINI, LEONARDO CASTELLANI, and PAOLO LOMELLINI

Enichem Polimeri, Mantova Research Center, Via Taliercio 14, 46100 Mantova, Italy

SYNOPSIS

An interpretation of yielding and fracture of rubber-toughened polymers is attempted, considering the fracture mechanics behavior of the matrices, with the rubber particles as stress-intensification sites. The fit of effective tensile yield stresses of composites vs. particle radii defines a stress-intensity factor K_{Yc} for craze yielding much smaller than the classical fracture factor K_c, and a critical particle radius for yielding. Different K_{Yc} values are found for polystyrene and poly(styrene-*co*-acrylonitrile)-based polymers. These factors are considered characteristic for craze initiation and propagation in the matrices, while K_c, in turn, would include also the craze-crack transformation contribution. K_{Yc} appears independent of the rubbery-phase volume fraction and characteristics, but two different values are found and discussed for poly(styrene-*co*-acrylonitrile)-based materials in two different particle-size ranges. A similar treatment on notched specimens' yield stress indicates the presence of a maximum in different radius ranges for polystyrene and poly(styrene-*co*-acrylonitrile) matrices, with higher values than their breakdown stresses. This stress increment is in relation to the minimum particle size inducing and still stabilizing crazes and preventing crack formation. This maximum seems to control the reinforcing extent of the polymer matrix conditioning the Izod fracture initiation energy.

INTRODUCTION

Yielding and impact strength in rubber-reinforced thermoplastic polymers have been widely studied in order to establish relationships with morphological and molecular parameters.[1,2] Nevertheless, ultimate properties can relate to the original morphological situation only in an indirect way, due to the strong structural changes induced by the plastic deformation before fracture.

Generalized or localized yielding is involved in both unnotched and notched fractures of rubber-toughened materials, and therefore the yielding process also has to be investigated to have a better insight into the impact behavior: The yielding should, in turn, be more directly related to the original structural situation.

Many investigations have been carried out on these topics by several authors, which have been partially reviewed in Ref. 3. Our previous results[3,4] on high-impact polystyrene (HIPS) and olephinic rubber-toughened styrene–acrylonitrile (OSA) show that

- The yield stress decreases, increasing the rubbery-phase volume and the particle size.
- The Izod energy increases, increasing the phase volume and the matrix molecular weight, and decreases, increasing the cross-linking degree of the rubbery phase.
- The Izod energy as a function of particle size shows a maximum in different positions for different rubber-toughened polymers; critical particle sizes below which the toughening efficiency vanishes were also observed.

These last results were obtained with a phenomenological approach by plotting the mechanical ul-

* To whom correspondence should be addressed.

Journal of Applied Polymer Science, Vol. 44, 505–520 (1992)
 CCC 0021-8995/92/030505-16$04.00

timate characteristics (Izod energy and yield stress) normalized "per single particle" against radius; the equations derived in this way gave families of Izod and of yield stress curves for different rubbery-phase volumes.

We adapt here from Ref. 3 the plot of the calculated Izod energy against the average rubber particle radius for HIPS and OSA (Fig. 1). The estimated minimum critical sizes were 0.065 μm for OSA and 0.29 μm for HIPS. For the yield stress of OSA, there was no mathematical evidence of a critical particle size; however, the particle effect below about 0.06 μm was practically zero (cf. Fig. 12 of Ref. 3). The same approach applied to the yield stress of a series of HIPS gives a critical particle size of about 0.4 μm.

Evidence of critical particle size for crazing have been reported,[5-9] supporting the idea that the particle size is one of the very controlling factors in the material's performance. The approach of Ref. 3 was rather phenomenological, and so the aim of the present work was to formulate hypotheses about the mechanism of yielding and to have more understanding about the possible relation to the impact resistance.

EXPERIMENTAL

Three different sets of rubber-toughened materials were considered: high-impact polystyrene (HIPS), olephinic rubber–styrene–acrylonitrile (OSA), and acrylonitrile–butadiene–styrene (ABS). The following characteristics, or some of them, were determined for the materials considered:

1. Rubbery-phase volume fraction by separation in selective solvents, centrifugation, and gravimetric determination.[3,4]
2. Average rubber particle radius by image analysis of TEM or optical micrographs.
3. Swelling index in toluene on HIPS according to the method described in Ref. 4.
4. Tensile modulus E and yield stress σ_y on type I dumbbell specimens, 3.2 mm thick with a crosshead speed of 5 mm/min according to ASTM D638.
5. Tensile tests on type I dumbbell specimens on 3.2 mm thick (ASTM D638) in which a notch according to ASTM D256 was machined (the crosshead speed was again 5 mm/min).

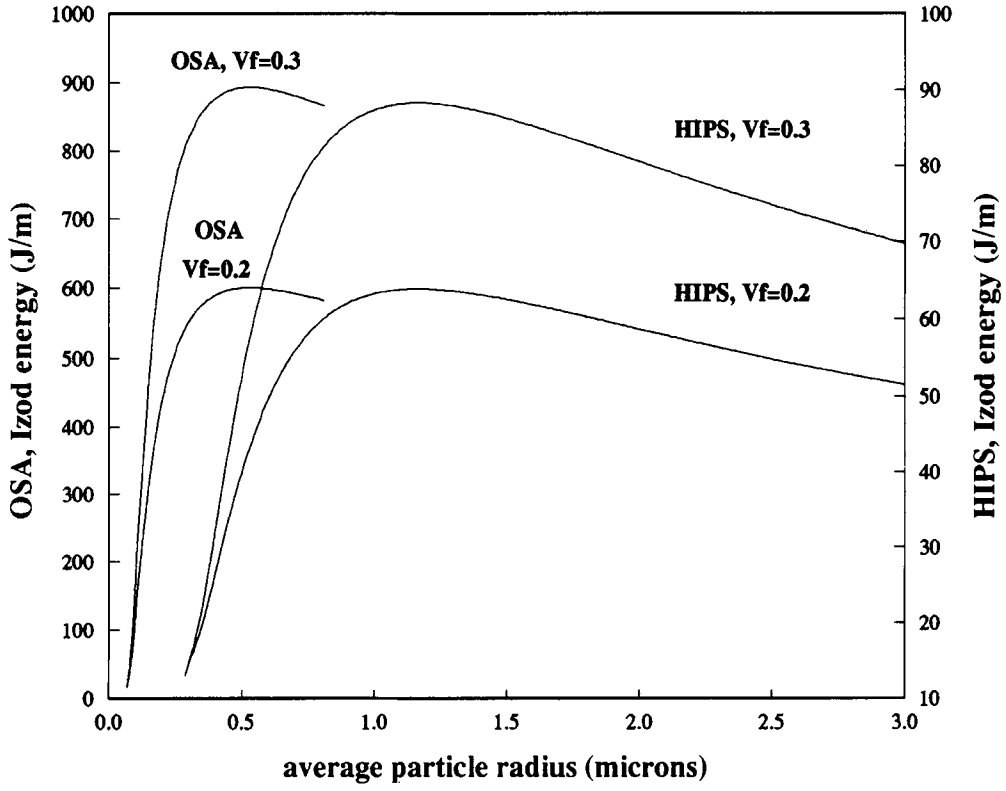

Figure 1 Calculated Izod energy (adapted from Ref. 3) vs. particle size for OSA and HIPS at two levels of rubbery-phase volume V_f.

6. Tensile tests on type I dumbbell specimens 3.2 mm thick (ASTM D638) unnotched and notched (notch according to ASTM D256) with different crosshead speeds ranging from 0.001 m/s to 1 m/s.
7. Notched Izod impact energy according to ASTM D256, test method A on 1/2 × 1/2 in. specimens.

Table I refers to the data for a series of HIPS (at constant cross-linking degree, swelling index about 10.5), OSA, and ABS. Rubbery volume fraction, particle radius, and tensile yield stress are reported.

Table II refers to a series of HIPS materials at different swelling indices, rubbery-phase content, particle size, tensile yield stress, Izod energy, and the parameter K_{Yc} (that will be discussed later) are also reported.

Table III reports, for some HIPS, OSA, and ABS materials, the Izod impact energy, the tensile modulus, and a reinforcing parameter that will be defined later.

The specimens for mechanical testing were obtained with two different procedures. In the first one, injection-molded plaques of the material were annealed in a compression-molding machine at 180°C for 5 min in order to have orientation-free samples. Finally, the specimens with the desired geometry were machined from the plaques. Compression molding of pellets was not used to avoid possible problems coming from poor welding of the pellets. This procedure was used for HIPS materials (H1–H23 in Table I) and for some specimens of OSA materials (O18–O22), namely, those used for the tensile tests at different crosshead speeds (Figs. 9 and 10).

In the second case, the mechanical testing was carried out on injection-molded specimens with the molding parameters chosen to have a small residual orientation. In general, this was more easily achieved for Izod specimens due to their large thickness. This procedure was used for all OSA and ABS materials of Table 1.

For some materials (H12, H17, H22; O18–O22), cross-checks between tensile tests on compression and injection-molded specimens were performed and the data agreement was satisfactory.

RESULTS AND DISCUSSION

Yielding

To understand the effects of the particle size on the yield stress, we tried to normalize the effect due to the rubbery-phase volume fraction. For a fixed par-

Table I Characterization Data for HIPS (H), OSA (O), and ABS (A) Samples (Yield Stress Measured at a Crosshead Speed of 5 mm/min)

Sample	Rubbery-Phase Volume Fraction	Particle Radius (μm)	Yield Stress (MPa)
H1	0.256	1.11	22.7
H2	0.278	1.44	21.8
H3	0.27	1.49	20.6
H4	0.306	1.57	20.0
H5	0.302	1.64	18.7
H6	0.274	1.07	24.6
H7	0.271	1.10	23.5
H8	0.267	0.99	26.4
H9	0.264	1.15	24.4
H10	0.292	1.49	22.0
H11	0.288	1.58	18.8
H12	0.285	1.72	17.8
H13	0.303	1.91	18.4
H14	0.137	1.13	28.7
H15	0.153	1.29	26.7
H16	0.136	1.05	31.2
H17	0.138	0.96	31.5
H18	0.141	1.35	25.9
H19	0.28	1.18	24.8
H20	0.375	1.38	19.2
H21	0.146	0.16	37.0
H22	0.155	0.18	37.5
H23	0.225	0.49	34.3
O1	0.413	0.081	35.0
O2	0.412	0.118	30.0
O3	0.45	0.124	23.7
O4	0.414	0.147	29.0
O5	0.375	0.145	32.5
O6	0.203	0.097	41.5
O7	0.203	0.083	43.5
O8	0.418	0.570	30.0
O9	0.407	0.124	30.6
O10	0.468	0.177	21.6
O11	0.313	0.118	35.0
O12	0.353	0.210	28.6
O13	0.337	0.147	34.0
O14	0.236	0.107	43.5
O15	0.352	0.222	26.5
O16	0.287	0.248	26.7
O17	0.441	0.270	16.7
O18	0.336	0.115	38.2
O19	0.412	0.125	30.8
O20	0.337	0.145	28.8
O21	0.427	0.160	24.5
O22	0.341	0.250	22.4
A1	0.33	0.095	38.0
A2	0.167	0.097	48.0
A3	0.202	0.344	48.0
A4	0.118	0.361	46.5
A5	0.153	0.483	44.4
A6	0.129	0.295	57.0
A7	0.203	0.560	33.0

Table II Characterization Data for HIPS Samples with Different Swelling Indexes

Sample	Rubbery-Phase Volume Fraction	Particle Size (μm)	Yield Stress (MPa)	Swelling Index	K_{Yc} (MPa · $\sqrt{m}$)	Izod Energy (J/m)
H24	0.130	1.27	23.5	8.8	0.029	38
H25	0.188	1.27	22.0	9.0	0.029	35
H26	0.265	1.27	19.0	8.9	0.026	55
H27	0.340	1.27	18.0	9.0	0.027	64
H28	0.115	1.67	23.0	10.5	0.032	38
H29	0.164	1.67	22.0	10.4	0.032	48
H30	0.246	1.67	20.0	10.6	0.031	63
H31	0.340	1.67	19.5	10.5	0.033	77
H32	0.158	1.73	21.0	12.6	0.031	48
H33	0.245	1.73	20.0	12.6	0.032	68
H34	0.265	1.73	19.8	12.0	0.032	75
H35	0.351	1.73	18.0	12.6	0.032	95
H36	0.379	1.73	17.5	12.4	0.032	101
H37	0.105	1.87	22.0	13.7	0.032	39
H38	0.151	1.87	20.0	13.7	0.031	56
H39	0.230	1.87	19.5	13.8	0.032	73
H40	0.254	1.87	19.0	13.9	0.032	86
H41	0.360	1.87	19.0	13.7	0.035	116
H42	0.112	1.87	21.5	17.0	0.032	46
H43	0.225	1.87	20.5	16.5	0.033	88
H44	0.307	2.00	18.5	16.6	0.033	120
H45	0.321	2.00	18.0	16.5	0.030	133

Table III Reinforcing Parameters for Various Materials

Material	Reinforcing Parameter	Izod Energy (J/m)	Tensile Modulus (MPa)
OSA	0.295	160	1960
OSA	0.437	290	1600
OSA	0.532	410	1850
OSA	0.484	650	1450
OSA	0.293	80	1550
OSA	0.461	410	1690
OSA	0.646	250	1730
OSA	0.612	120	2390
OSA	0.431	400	1770
HIPS	0.068	85	1400
HIPS	0.017	75	1100
HIPS	0.067	28	2500
HIPS	0	26	2600
ABS (small particle)	0.835	401	1900
ABS (large particle)	0.370	250	1800
ABS (small particle)	0.558	180	2610
ABS (small particle)	0.620	320	1720
ABS (large particle)	0.491	140	2800
ABS (small particle)	0.548	90	2750
ABS (large particle)	0.458	125	1810
ABS (large particle)	0.117	130	1000

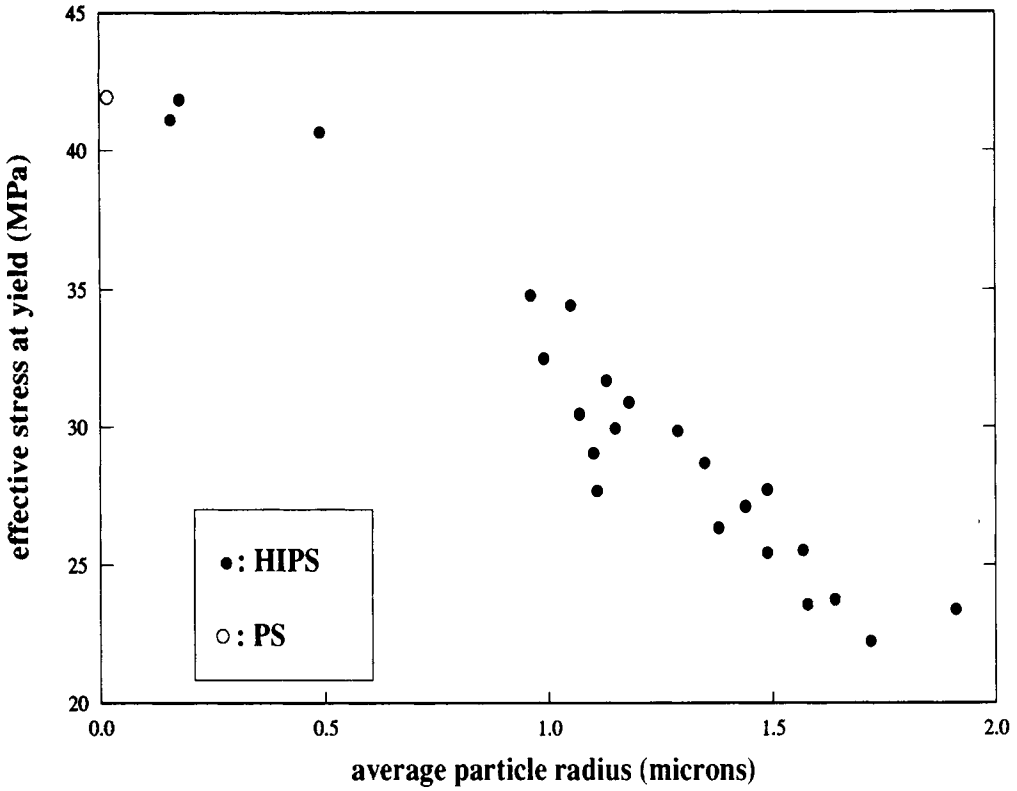

Figure 2 Effective yield stress vs. particle size for the HIPS series of Table I. The breakdown stress of PS is also indicated.

ticle size, the yield stress decrease with increasing second-phase volume content in ABS has been shown to depend only on the effective matrix cross-sectional area reduction due to the presence of the rubber particles[10]; a simple formula first developed for compressive yielding of epoxy composites by Ishai and Cohen was used.[11] This formula is based on a calculation of the reduced cross section assuming homogeneously sized particles arranged in a cubic lattice.

To avoid any assumption about spatial arrangement and the morphological characteristics of the dispersed phase, we adopt the simple equation

$$(\sigma_y)_e = \frac{\sigma_y}{(1-\phi)^{2/3}} \qquad (1)$$

where σ_y is the yield stress referred to the total specimen cross section, ϕ is the second-phase volume fraction, and $(\sigma_y)_e$ is the normalized yield stress that we will call effective yield stress.

Considering that in a specimen of volume V the volume occupied by the matrix is $V(1-\phi)$, then eq. (1) comes from the application of the factor $(1-\phi)^{1/3}$ to all the linear dimensions of the specimen, thus obtaining $(1-\phi)^{2/3}$ as a reducing factor for the cross-sectional area.

Figure 2 shows a plot of $(\sigma_y)_e$ vs. the average particle radius R for HIPS materials. In Figure 2 it is possible to notice that the effective values of the yield stress $(\sigma_y)_e$ are never higher than the macroscopic bulk breakdown stress of the polystyrene (PS) matrix, $\sigma_m^{(PS)}$ (see Table IV).

Using the Isahi–Cohen normalization would lead

Table IV Parameters for PS- and SAN-Based Materials

Materials	Matrix K_c (MPa·$\sqrt{m}$)	K_{Yc} (MPa·$\sqrt{m}$)	R_c for Izod (Ref. 3) (μm)	R_c for Yielding (Eq. 3) (μm)	σ_m (MPa)	σ_m^N (MPa)	$\frac{(\sigma_m - \sigma_m^N)}{\sigma_m^N}$
PS-based	1	0.032	0.29	0.58	42.2	30.7	0.37
SAN-based (large particles)	1.6	0.031	—	0.25	62.0	27.7	1.24
SAN-based (small particles)	1.6	0.015	0.065	0.07	62.0	27.7	1.24

in many cases to the rather unrealist finding of $(\sigma_y)_e$ values much higher than the breakdown stress of the PS matrix. This is a further argument to support our proposed normalization.

Moreover, a strong dependence of $(\sigma_y)_e$ on R can be easily observed; this is hard to understand in terms of stress concentration around spherical soft inclusions[12] only. To account for this dependence on R, we assume that craze propagation from the matrix–particle interface occurs according to the linear elastic fracture mechanics (LEFM) criteria that describe the propagation of cracks in linear elastic bodies. We identify the onset of craze propagation with the macroscopic yielding, and we make the further assumption that the defects which originate craze propagation (which have to be considered, in the LEFM framework, preexisting to the propagation itself) have the same linear dimensions of the rubbery particles. We then introduce a factor K_{Yc} that relates the critical effective stress for the onset of craze yielding with the rubber particles radius R through the following equation:

$$(\sigma_y)_e^2 = \frac{K_{Yc}^2}{R} \qquad (2)$$

Equation (2) mimics the basic fracture mechanics relationship between the stress for the crack initiation and the dimension of the flaw.[13]

We do not attempt to model the detailed process of nucleation of the above-mentioned defects, and we do not make hypotheses about their shape; Therefore eq. (2) does not contain an explicit assessment of a geometric factor and the factor K_{Yc} has only a semiquantitative meaning. This equation was found to fit the experimental data in a satisfactory way, with different values of K_{Yc} corresponding to different groups of materials.

Figure 3 shows a linear regression, forced through the origin, of the squared effective yield stress vs. the reciprocal particle size for HIPS. All PS-based materials data are fitted by eq. (2) with a single value of K_{Yc}. Figure 4 reports the same data of Figure 3 in terms of the effective yield stress vs. the particle size (the breakdown stress of the matrix is also indicated). On the other hand, Figure 5 shows that the data for styrene–acrylonitrile (SAN)-based materials split into two groups, each fitted by a different value of K_{Yc}.

The three regression curves and the values of breakdown stresses for the two matrices ($\sigma_m^{(PS)}$ and

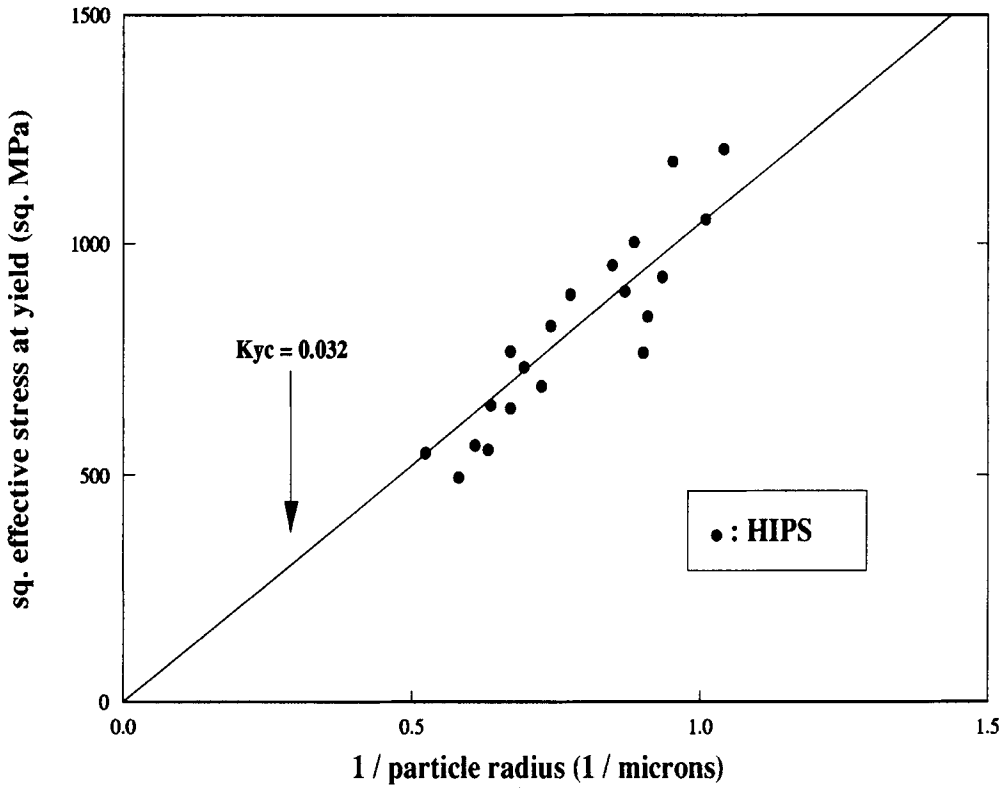

Figure 3 Linear regression of the effective yield stress vs. the reciprocal particle size for the HIPS series of Table I. The three samples, H21, H22, and H23, with the lowest radii are not included in the regression (see also Fig. 4).

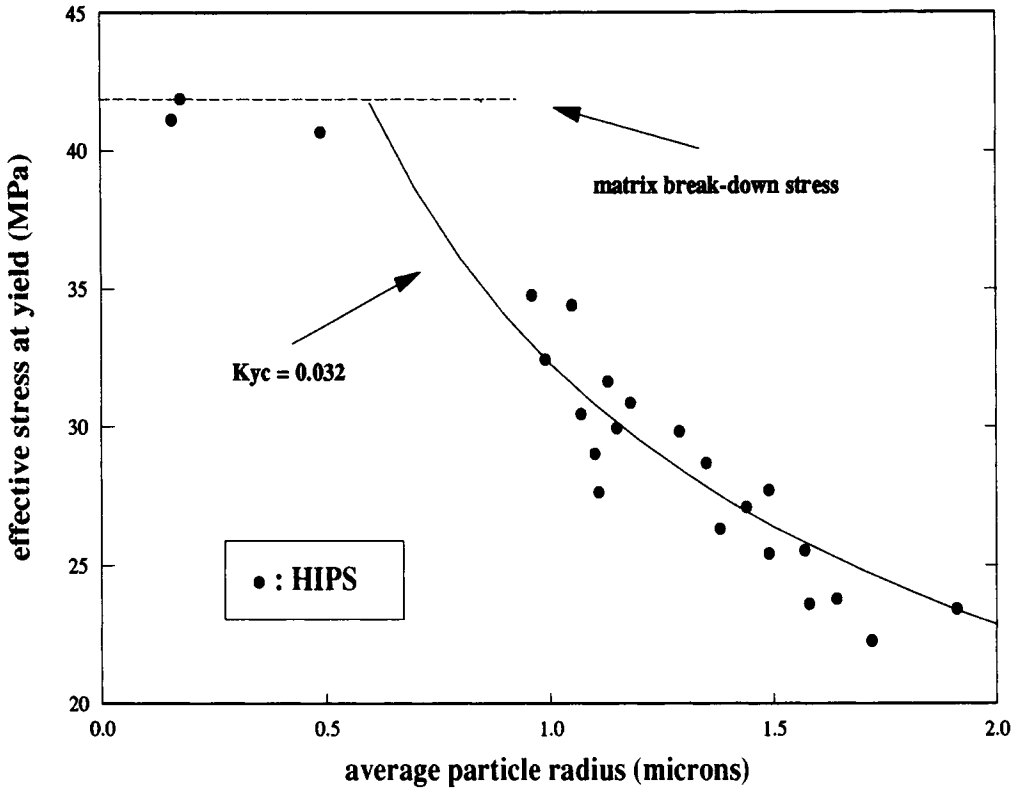

Figure 4 Effective yield stress vs. particle size for the HIPS series of Table I. The regression curve obtained by Figure 3 is also reported.

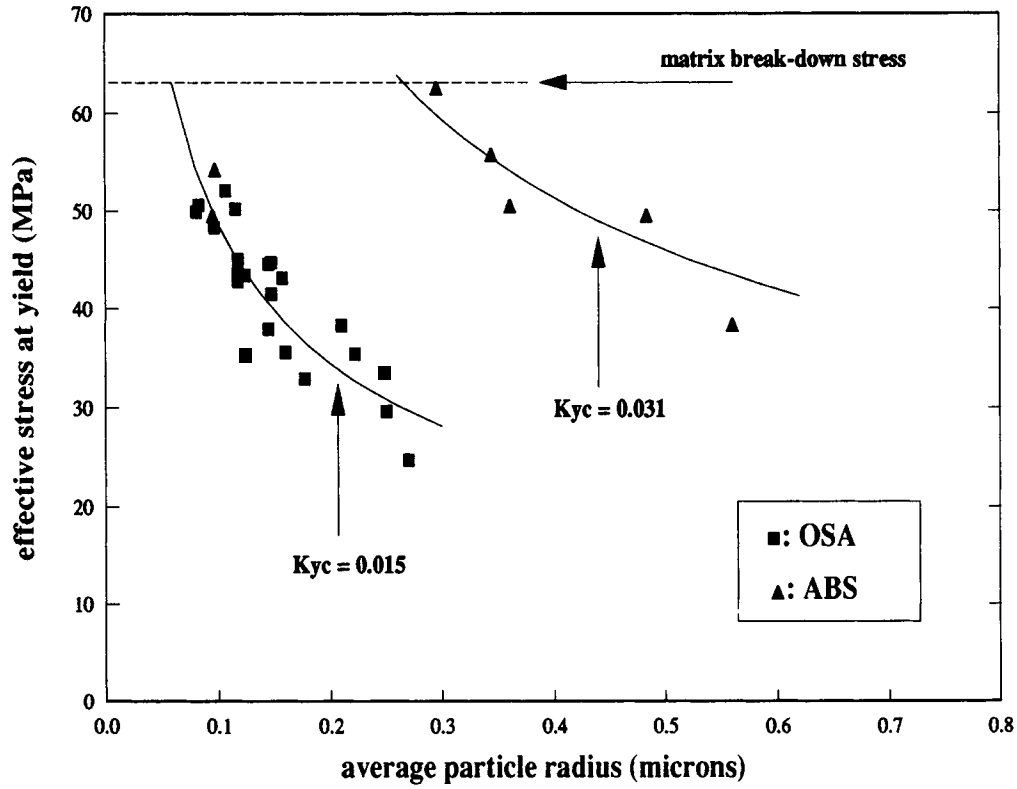

Figure 5 Same as Figure 4 for SAN-based materials.

$\sigma_m^{(SAN)}$) are shown together in Figure 6. The three values of K_{Yc} and the stress intensity factors K_c of PS and SAN from Ref. 13 are reported in Table IV.

The fact that the values of K_{Yc} are far smaller than the stress intensity factors K_c for the correspondent matrices is not completely unexpected and can be justified considering that the energy required for craze nucleation and propagation is likely to be lower than that for fracture. Fracture energy in craze-prone polymers, in fact, results not only from craze nucleation and propagation, but, also, for example, from the fibril breakdown process. Rubber particles have been shown to act as craze terminators,[1] thus inhibiting fibril breakdown at least during the earliest stages of yielding. The parameter K_{Yc}, which comes from yield stress data, should therefore be related to craze nucleation and propagation but not to fibril breakdown.

Equation (2) holds is validity only when the effective stress is lower than the breakdown stress of the matrix or, which is equivalent, when the average particle radius is above a critical radius R_c (see Table IV), which is defined by the following simple equation:

$$R_c = \left(\frac{K_{Yc}}{\sigma_m}\right)^2 \qquad (3)$$

The definition above could have been more elegant if we had chosen the stress for the craze nucleation in the matrix instead of the breakdown stress, which is, in general, higher and influenced by molecular parameters not affecting the first one. However, in our case, the difference between these two values has been ignored, considering it of minor importance.

Because of the fact that the yield stresses of the matrix and of the rubber-modified materials depend on the test parameters, like, for example, the strain rate, and on the materials' characteristics, like the matrix molecular weight, the values of K_{Yc} and of R_c should be, in principle, affected by the same variables. On the other hand, the structural characteristics of the rubbery phase, like the degree of crosslinking, do not play a significant role, as will be shown later.

Yielding of SAN-Based Materials

We already showed in Figure 5 that rubber-toughened SANs having very different particle size can exhibit the same effective yield stress. As mentioned before, this leads to two different curves and two K_{Yc} values for SAN-based materials: One is related

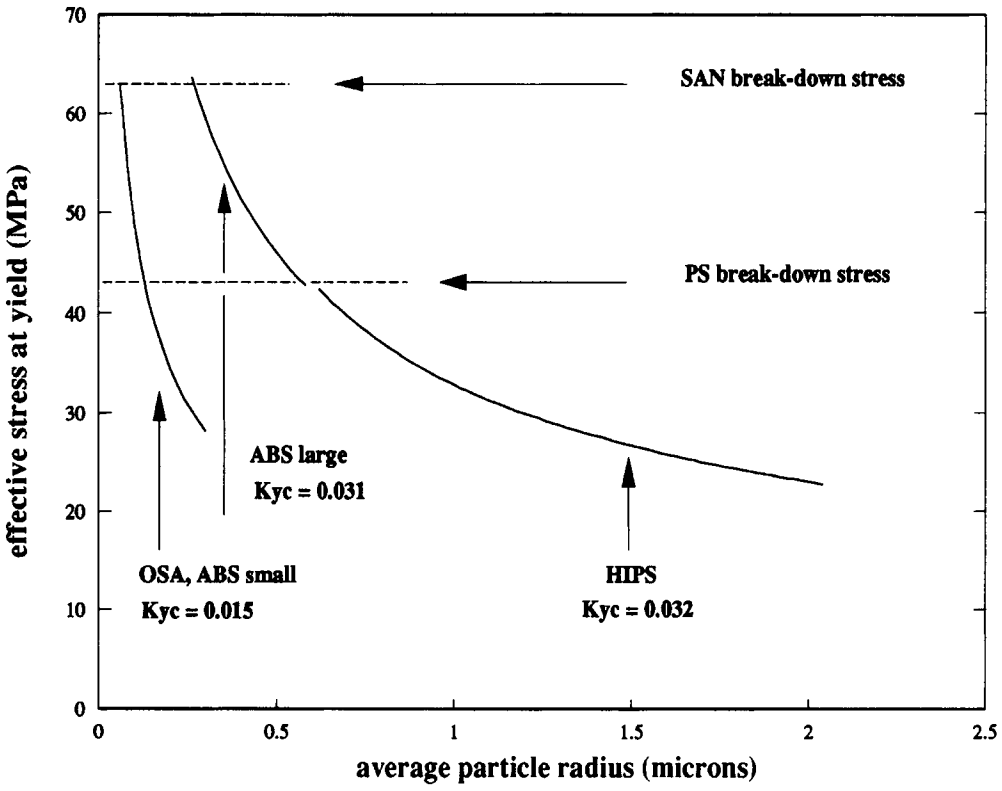

Figure 6 Regression of the effective yield stress vs. particle size for the three material groups.

to OSA and ABS with small particles; the other, to ABS with big particles. The indicators 1 and 2 hereafter refer to the first and the second group of materials, respectively.

The rubbery-phase particles do not all have exactly the same internal structure: In group 1, there are materials containing polybutadienic "bulk rubber" particles (A1 and A2) and olephinic "salamilike" particles (O1–O22), whereas materials in group 2 contain only polybutadienic "salamilike" particles (A3–A7). Because the rubbery-phase internal structures of the materials in the first group are not homogeneous, it seems tentatively reasonable to think that the rubbery-phase characteristics should not be invoked to account for the existence of two different values of K_{Yc}.

In fact, the approach we followed deals only with the yielding characteristics of the matrices, considering that the rubber particles simply modify the stress geometry. The presence of two different K_{Yc} values for the toughened SANs appears therefore to be related to the occurrence of two different yielding mechanisms triggered by pure morphological reasons. The effects of the particle size on plastic deformation mechanisms have been investigated in the literature, showing that the decrease of size increases the shear contribution.[5,7,9]

For the SAN-based materials of Table I, it is also possible to compute the values of the mean interparticle free distance (MFD) through the following formula:

$$\text{MFD} = \frac{1 - \phi}{3\phi} \cdot R \qquad (4)$$

As a matter of fact, the materials in group 1 all have lower MFDs than 0.23 μm, whereas the values of MFD for the materials in group 2 are higher. It is possible then that the MFD represents a critical parameter for the yielding mechanisms distinguishing the two groups. The importance of a critical interparticle distance (ID), which is, in principle, similar to the MFD, was first discussed for the ductile-brittle transition in notched impact tests of rubber-toughened nylons.[14–16] As far as we know, for that class of materials, the interparticle distance was not reported to be a critical factor for the tensile yield stress; we cannot therefore easily conclude that a strong similarlity with our case exists. However, as suggested by Wu,[17] in rubber-toughened polymers, large IDs should be associated to a plane strain situation, whereas a small ID can induce a plane stress state in the matrix. Considering that Sternstein and Ongchin[18] indicated that the transition from crazing to shear yielding is possible with changes in stress geometry, the reduction in MFD could be interpreted as a key factor favoring the shear-yielding contribution.

Despite the fact that the suggested interpretation of the two K_{Yc} curves for SAN in terms of the crazing–shear-yielding balance is appealing, the experimental results do not completely elucidate this hypothesis. The strong decrease of the yield stress on going from group 2 to group 1 materials is hard to believe as explained simply by the reduction of the crazing contribution to the yielding mechanism. The reported considerations are then not conclusive and a more detailed investigation is needed.

Yielding of Notched and Unnotched Specimens

In this section, we are going to consider the data about tensile tests on notched specimens. Referring to these, we will call the notched yield stress σ_y^N the one computed from the maximum in the load-extension curves. In doing this, we took into account the minimal specimen section in the notch region. Stresses obtained in this way were then normalized according to the procedure described above [eq. (1)] in order to obtain the values of the effective yield stress of the notched samples $(\sigma_y^N)_e$. Samples without the rubbery phase were also tested in the same way. Hereafter, the breakdown stress of matrix notched specimens will be referred to as σ_m^N.

Figures 7 and 8 show the stress-displacement curves for notched and unnotched specimens of materials O22 and O18, respectively, at a crosshead speed of 0.1 m/s. It is possible to observe that in one case the maximum stress is practically notch-insensitive, whereas in the other case, the presence of the notch strongly depresses the maximum load borne by the material.

Figure 9 reports the values of $(\sigma_y)_e$ and of $(\sigma_y^N)_e$ vs. R for some OSA, together with the value of σ_m and of σ_m^N of its matrix. The following features can be observed:

1. For large-particle radii, the values of $(\sigma_y^N)_e$ and of $(\sigma_y)_e$ are quite similar.
2. Decreasing the particle radius, the value of $(\sigma_y^N)_e$ tends to be lower than that of $(\sigma_y)_e$ but higher than σ_m^N; in this range, a value of R exists, which we will call R_{max}, for which $(\sigma_y^N)_e$ exhibits a maximum $(\sigma_{max}^N)_e$.
3. For particle radii lower than the critical radius R_c, $(\sigma_y^N)_e$ is approximately equal to σ_m^N.

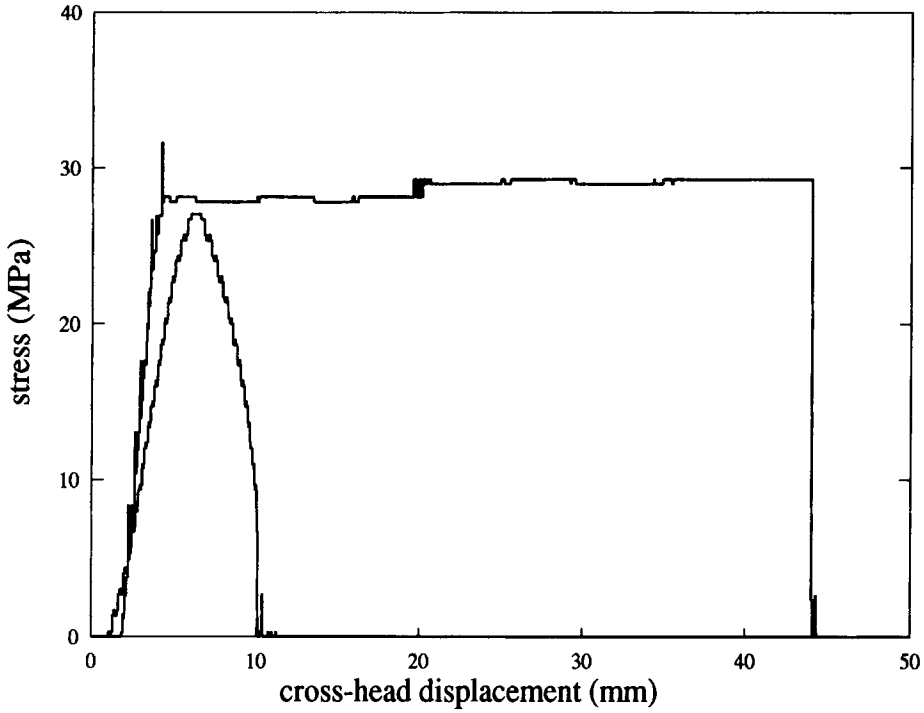

Figure 7 Stress-displacement curves for notched and unnotched specimens of material O22 with a crosshead speed of 0.1 m/s. The bell-shaped curve refers to the notched specimen.

This last feature is not easy to be confirmed for OSA as it would require materials with very small radii. However, we checked it with two HIPS samples with particle radii (0.16 and 0.18 μm) smaller than R_c. Their $(\sigma_y^N)_e$ (30 and 32 MPa) are quite similar to the value of σ_m^N of the PS (30.7 MPa).

This scheme should be considered as qualitative because, in the case of notched specimens, at the notch tip there is the effect of an increased strain rate and of a triaxial state of stress that can have an influence on the absolute values of $(\sigma_y^N)_e$.

In any case, Figure 10 shows that the trend of Figure 9 is observed in a wide range of strain rates; furthermore, it is reasonable to suppose that the effect of stress triaxiality is particle-size independent. Thus, the shape of $(\sigma_y^N)_e$ vs. particle should not be modified by the two effects mentioned above.

This behavior can be interpreted in terms of the competition between the effects of the particles and of the notch on the yielding mechanisms. When the particle radius is large enough to produce a low effective stress at yield, the mechanism of yielding takes place in the material as if the notch were absent. We can introduce here the critical value R_c^N:

$$R_c^N = \left(\frac{K_{Yc}}{\sigma_m^N}\right)^2 \tag{5}$$

Of course, because of the fact that the value σ_m^N depends on the notch characteristics and tends to be lower when the notch is more sharp, R_c^N is a more complex parameter than R_c, its value depending not only on the matrix characteristics and on the test parameters, but also on the notch geometry.

Above R_c^N, the behavior of notched and unnotched specimens is essentially the same. When the particle size is lower than R_c^N, one could expect, in analogy with the case of the unnotched specimens, that the effective stress has reached its maximum, the notch effect being prevalent on the yielding. However, the observed effective stresses are still similar to the unnotched case for a certain particle-size range below R_c^N. Decreasing further the particle size, the effective yield stress shows a maximum at an intermediate value between σ_m^N and the unnotched σ_m.

The presence of this maximum stress can be explained invoking the fact that the two-phase material has, at the notch tip, different characteristics from the matrix. We can assume, in fact, that the rubber particles, together with the craze-initiation effect discussed above, can promote, in some way, the stabilization of the crazes that form at the notch tip and that would induce the brittle fracture in the notched matrix. The efficiency of the particles in

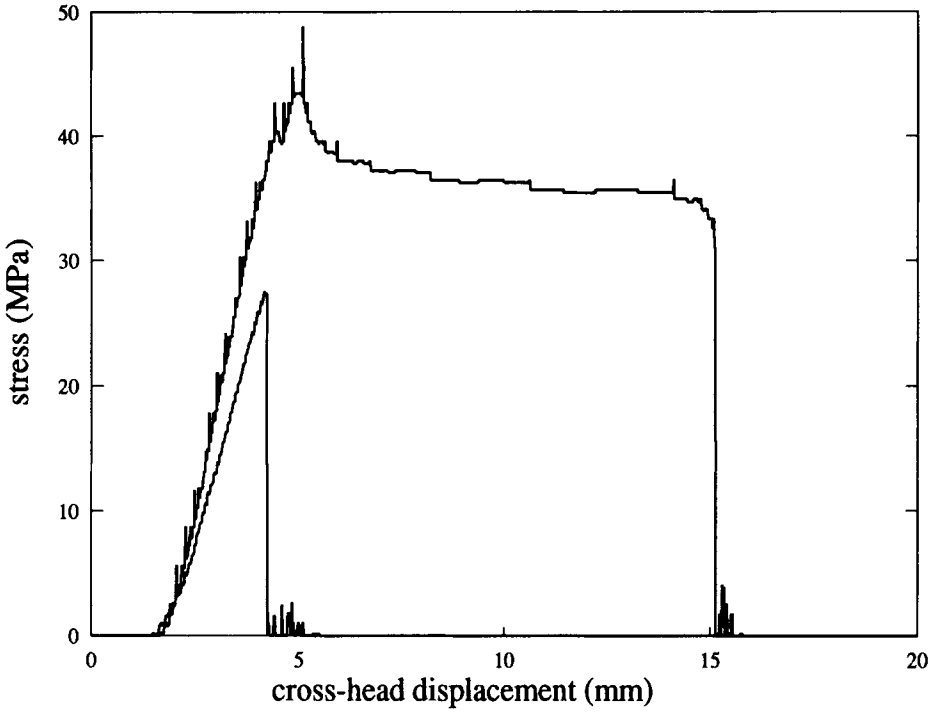

Figure 8 Stress-displacement curves for notched and unnotched specimens of material O18 with a crosshead speed of 0.1 m/s. The lower curve refers to the notched specimen.

stabilizing the crazes depends on their size and tends to decrease, approaching the critical radius R_c, below which no yielding is favored by the rubber particles and the effective stress of the rubber-toughened material coincides with the breakdown stress of the notched matrix.

The radius R_{max} and the maximum effective stress σ^N_{max} for notched specimens, which are then determined by the combined effects of the yielding and of the notch, depend, of course, on the same parameters that influence R_c and R_c^N already mentioned. Furthermore, taking into account the fact that the experimentation concerning the notched specimens is not as exhaustive as the one about unnotched samples, we cannot be sure "*a priori*" that the normalization of the stress values made by eq. (1) also eliminates completely the second-phase effects in this case and then we cannot exclude that the rubbery volume fraction affects slightly R_{max} and the corresponding stress. Similarly, we cannot be sure that the cross-linking or, more in general, the rubbery-phase characteristics do not influence the shape of the curve collecting the data for the notched specimens. It is then possible, in principle, that the position and the value of the maximum of the effective stress can be affected by these parameters. However, for the yield process, it seems reasonable that rubbery-phase features other than particle size should play a secondary role.

Considerations About Izod Energy

It is interesting at this point to note a similarlity in the shapes of plots of the notched tensile yield stress at different tests speed (Figs. 9 and 10) and of the notched Izod resistance (Fig. 1) vs. particle radius. As pointed out before, the notched yield stress in tensile tests represents the maximum stress that the materials can bear before the crack propagation. The fracture initiation energy is then likely to be controlled by this value of stress and it is possible that the dependence of the initiation energy from the particle radius is analogous to that of the effective notched yield stress. However, the Izod resistance contains, together with a fracture initiation contribution, also a fracture propagation part, which can be nonnegligible.

Our previous work[14] shows a strong effect of the rubbery-phase degree of cross-linking on the Izod energy, particularly on the contribution due to the propagation. Evidence for that can be also observed in Figure 11, where Izod data (normalized per single particle according to Ref. 3) for HIPS samples sam-

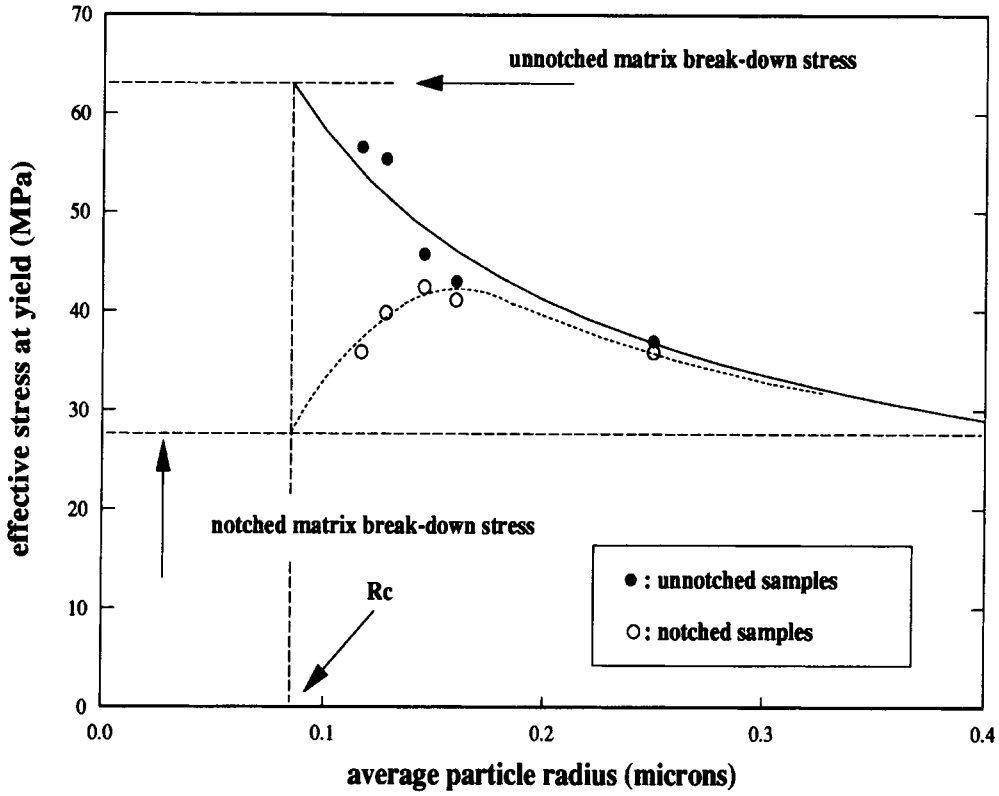

Figure 9 Effective yield stress in notched and unnotched specimens of some OSA materials. Crosshead speed 0.1 m/s. The continuous line refers to an estimated K_{Yc} value of 0.018 MPa $\cdot \sqrt{m}$.

ples are plotted vs. the swelling index. The swelling index is known to be a measure of degree of cross-linking, its value increasing as the cross-linking density decreases. On the other hand, calculating the K_{Yc} values (see Fig. 12) for a series of HIPS with different levels of cross-linking (Table II) shows a substantial constancy of this parameter (0.031) at the same level found for the previously described HIPS series (0.032), reinforcing the idea of the independence of the K_{Yc} on the rubbery-phase characteristics.

It is therefore clear that a strong relationship between the notched Izod energy and the yielding of notched specimens is not expected; however, the latter should reasonably be related to the fracture initiation contribution to the Izod energy.

What seems interesting is that both the effective notched yield stress and the Izod resistance tends to show a minimum critical particle size (as the effective unnotched yield stress does) and they reach a maximum again as a function of the particle radius (Table IV). Of course, the values of these radii are not strictly the same in the two cases, this fact depending both on the nature of the two tested parameters and on the different test conditions. Anyway, the information coming from the analysis of the yielding in notched and unnotched specimens can, in our opinion, be useful to predict approximately the toughenability of the matrix (or at least the initiation energy contribution to the fracture) and the optimum particle-size range. The radii R_c and R_c^N that we defined in the previous sections can be considered, for instance, as the borders of that range.

We suppose that, at a given notch geometry, the toughenability of the matrix increases when its yielding resistance factor K_{Yc} is lower and when the fracture resistance parameters of the matrix (like σ_m or $[\sigma_m - \sigma_m^N]$ or $[(\sigma_m - \sigma_m^N)]/\sigma_m^N$) are higher. Consider, for instance, the last parameter to be representative of the maximum matrix toughenability: It has values of about 0.37 and 1.24 for PS and SAN, respectively, in agreement with the well-known fact that SAN-based materials are tougher than PS-based ones.

In this scheme, we suppose that $[(\sigma_y)_e^N - \sigma_m^N]/\sigma_m^N$ should be a kind of reinforcing efficiency parameter of the rubber-modified material. The product of Izod energy and elastic modulus vs. this reinforc-

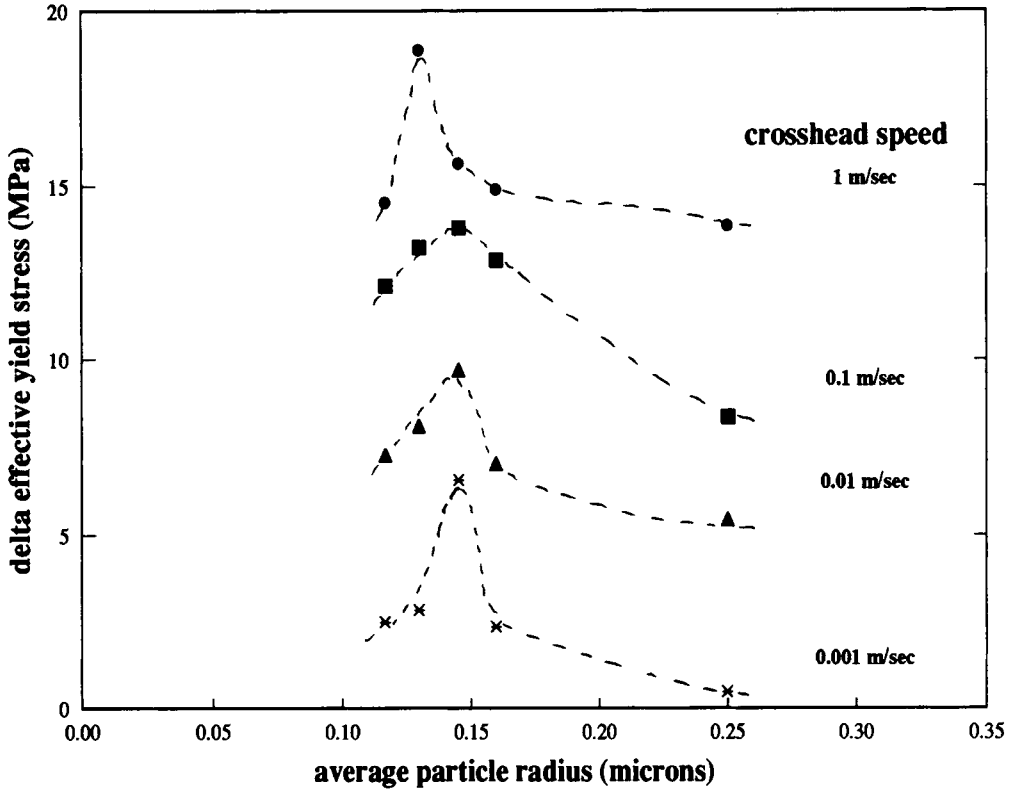

Figure 10 Effective yield stress of some OSA samples at different crosshead speeds. The corresponding σ_m^N values have been subtracted from each curve.

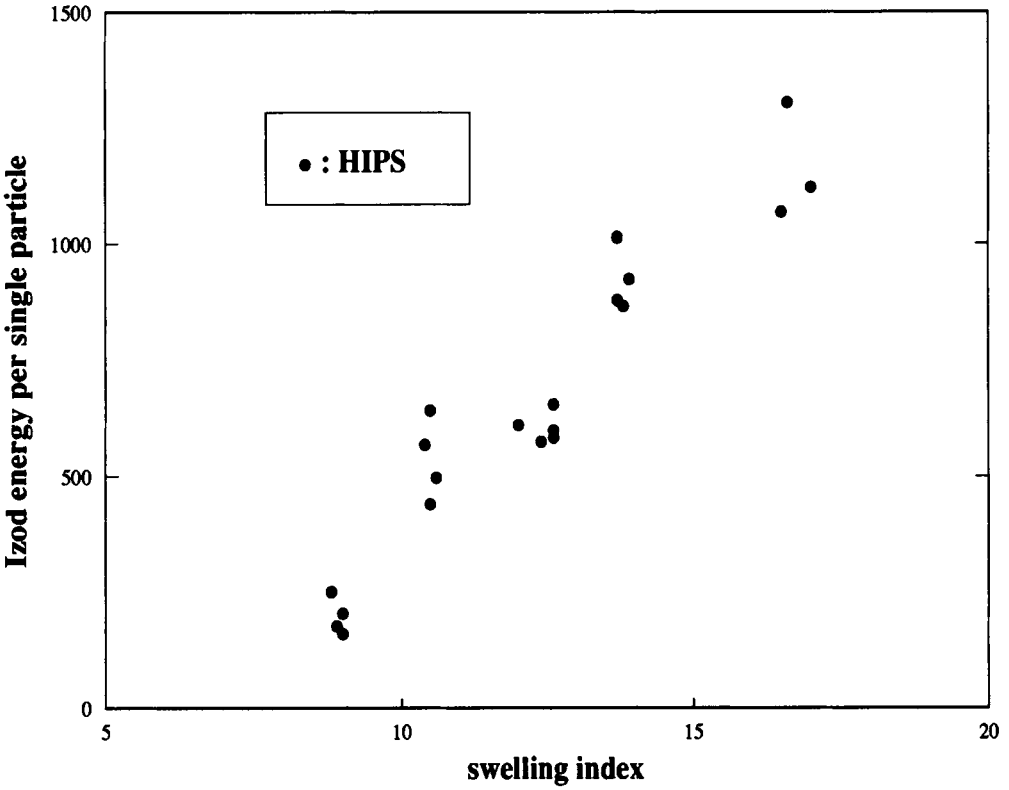

Figure 11 Izod energy normalized per single particle (according to Ref. 3) vs. swelling index for the HIPS series of Table II.

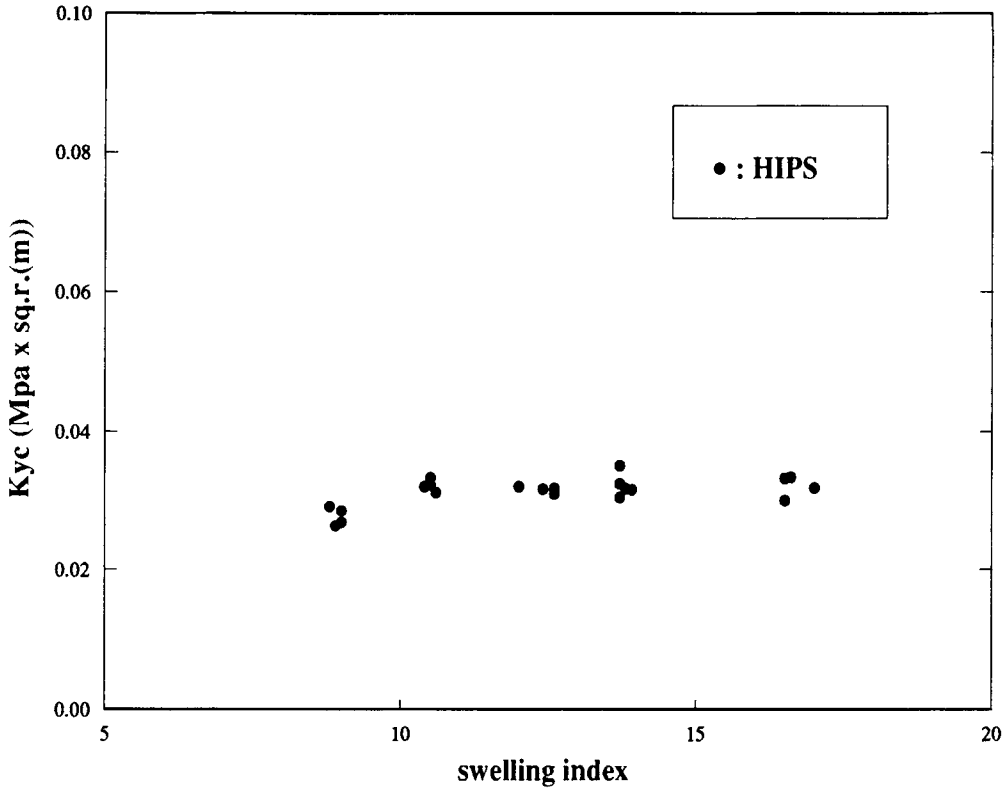

Figure 12 K_{Yc} values vs. swelling index for the HIPS series of Table II.

ing parameter is shown in Figure 13 for a group of materials having different matrices, rubbery-phase content, and characteristics. The Izod values were multiplied by the modulus, which is equivalent, to normalize the Izod per unit compliance. This approach also removes, at least in a first approximation, the rubbery–phase effect on the Izod itself, as the opposite rubbery-phase effect on the yield stress was removed with eq. (1). Although, a rather large data scatter, as expected, is observed, it is possible to notice an increasing trend. The dashed lower line drawn could represent a lower limit approximately related to the fracture initiation energy. PS-based materials are also observed to be confined in a range of both parameters that is smaller with respect to SAN-based materials. This is consistent with the idea that the maximum toughenability parameter, $[(\sigma_m - \sigma_m^N)]/\sigma_m^N$, for PS-based materials (0.37) is lower than that of SAN-based ones (1.23).

Of course, the parameters introduced in this section have to be considered only as qualitative indications. For example, the shape and the position of the maximum of the Izod curves (Fig. 1) and those of the notched yield stress curves (Figs. 9 and 10) are not the same. Furthermore, for some HIPS materials with large particles, it is possible to have a negative reinforcing efficiency parameter but still an improvement of the Izod energy with respect to the matrix.

A more detailed experimentation (e.g., measurements of fracture initiation energy) and more precise theoretical considerations (about the stress state around a particle or an intrinsic defect or a notch) should be done to get a more quantitative assessment of the ideas we inferred in this simple approach.

CONCLUSIONS

The behavior at yielding appears to be controlled substantially by two parameters:

(i) the breakdown stress of the matrix with and without notch (σ_m and σ_m^N, respectively);
(ii) the factor K_{Yc} defined in the eq. (2) and related to the mechanisms of yielding taking place in rubber-modified materials.

As previously pointed out, the value of σ_m and σ_m^N cannot be considered constant without keeping fixed all the test parameters, from the specimens preparation to the test conditions. These can also

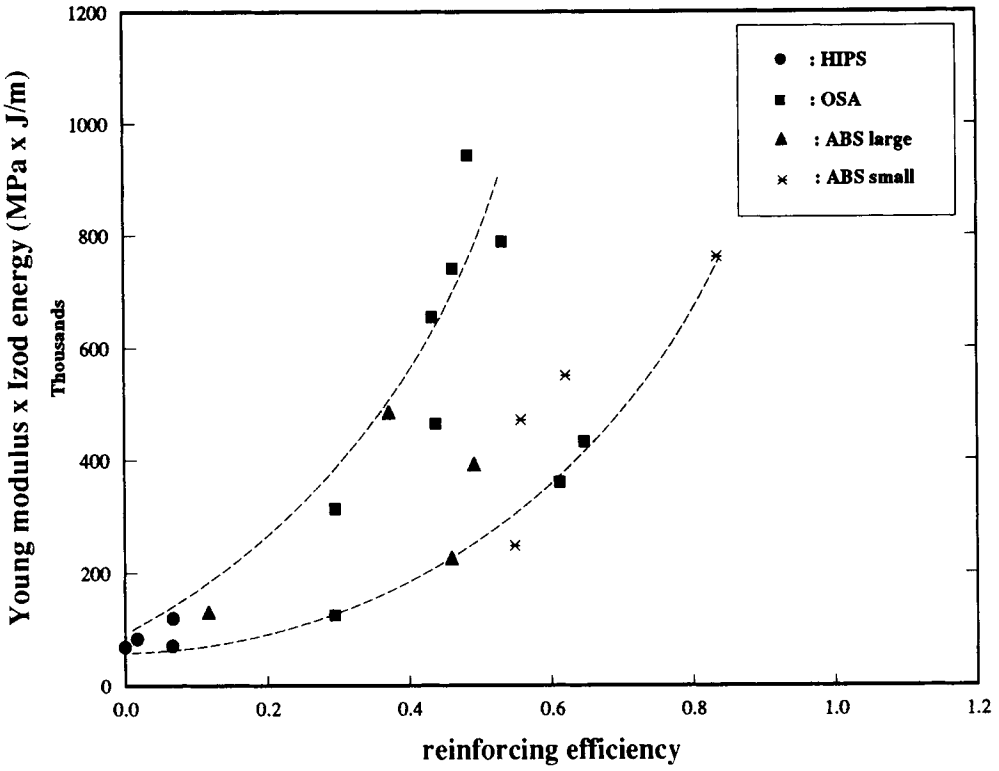

Figure 13 Izod energy and Young modulus product vs. the reinforcing efficiency (see text) for the materials of Table III.

affect the K_{Yc} values. However, we believe that these parameters describe reasonably well the influence of the morphology on the mechanisms of yielding. A direct consequence of the approach that we followed is the possibility to define a critical particle radius R_c below which the effects of the rubbery phase on the yielding mechanism disappear.

The presence of a notch modifies significantly the materials' behavior, and we tried to understand this behavior examining how the presence of the notch influences the yielding mechanism. We considered the breakdown stress for the notched matrix and defined a critical particle radius R_c^N in the same way that we followed in the definition of R_c. It is then possible to separate three different ranges of particle radius corresponding to three very different behaviors exhibited by the notched specimens:

- For large-particle radii, the notch is ineffective and the yielding takes place controlled only by the same mechanisms existing in the unnotched specimens.
- When R decreases and approaches R_c, the yielding mechanisms are influenced by the presence of the notch that tends to be more relevant as far as the particle size decreases. In this region, the effective stress, considered before the crack formation at the notch tip, exhibits a maximum $(\sigma_{max}^N)_e$ corresponding to a particle radius R_{max}.
- For $R < R_c$, the particle effects vanish and the notch is the key factor controlling the materials' performance, which is substantially similar to that of the notched matrix.

It is interesting to conclude that the two matrix parameters σ_m^N and σ_m are strictly related to the range of the efficient particle size; in fact, it is easy to conclude from the eqs. (3) and (5) that

$$\frac{\sigma_m}{\sigma_m^N} = \sqrt{\frac{R_c^N}{R_c}} \tag{6}$$

On the other hand, the maximum stress $(\sigma_{max}^N)_e$ should reasonably be higher when the matrix breakdown stress σ_m is high and when R_{max} is close to R_c, that is, when the craze stabilizing efficiency of the particles is retained at small R values. Furthermore, it is reasonable to assume that this maximum effective stress $(\sigma_{max}^N)_e$ is related to the toughenability of the matrix.

REFERENCES

1. C. B. Bucknall, *Toughened Plastics,* Applied Science, London, 1977.
2. C. K. Riew, Ed., *Rubber Toughened Plastics, Adv. Chem. Ser.,* **222** (1989).
3. G. Cigna, P. Lomellini, and M. Merlotti, *J. Appl. Polym. Sci.,* **37,** 1527 (1989).
4. G. Cigna, S. Matarrese, and G. F. Biglione, *J. Appl. Polym. Sci.,* **20,** 2285 (1976).
5. A. M. Donald and E. J. Kramer, *J. Mater. Sci.,* **17,** 1765 (1982).
6. A. M. Donald and E. J. Kramer, *J. Appl. Polym. Sci.,* **27,** 3729 (1982).
7. J. N. Sultan and F. J. McGarry, *Polym. Eng. Sci.,* **13,** 29 (1973).
8. S. Y. Hobbs, *Polym. Eng. Sci.,* **26,** 74 (1986).
9. B. Z. Jang, D. R. Uhlmann, and J. B. Vandersande, *J. Appl. Polym. Sci.,* **30,** 2485 (1985).
10. T. Ricco, M. Rink, S. Caporusso, and A. Pavan, in *Toughening of Plastics II,* Proc. Int. Conf., London, 1985.
11. O. Ishai and L. J. Cohen, *J. Comp. Mater.,* **2,** 302 (1968).
12. J. N. Goodier, *J. Appl. Mech.,* **55,** 39 (1933).
13. J. G. Williams, *Fracture Mechanics of Polymers,* Ellis Horwood, Chichester, 1984.
14. R. J. Borgrreve, R. J. Gaymans, J. Schuijer, and J. F. Ingen Housz, *Polymer,* **28,** 1489 (1987).
15. R. J. Borgrreve, R. J. Gaymans, and A. R. Luttmer, *Makromol. Chem. Makromol. Symp.,* **16,** 195 (1988).
16. S. Wu, *Polymer,* **26,** 1855 (1985).
17. S. Wu, *J. Appl. Polym. Sci.,* **35,** 549 (1988).
18. S. S. Sternstein and L. Ongchin, *ACS Polym. Prep.,* **10,** 1117 (1969).

Received February 12, 1991
Accepted April 8, 1991